Radiochimica Acta 73, 55–66 (1996)

On-line Gas Phase Chromatography with Chlorides of Niobium and Hahnium (Element 105)

By A. Türler, B. Eichler, D. T. Jost, D. Piguet
Paul Scherrer Institut, CH-5232 Villigen PSI, Switzerland

H. W. Gäggeler
Paul Scherrer Institut, CH-5232 Villigen PSI, Switzerland and
Labor für Radio- und Umweltchemie, Universität Bern, CH-3012 Bern, Switzerland

K. E. Gregorich, B. Kadkhodayan, S. A. Kreek, D. M. Lee, M. Mohar, E. Sylwester, D. C. Hoffman
Lawrence Berkeley Laboratory, Berkeley CA 94720, USA

and S. Hübener
Institut für Radiochemie, Forschungszentrum Rossendorf, D-01314 Dresden, Germany

(Received October 12, 1995; accepted February 16, 1996)

On-line gas chromatography / Group 5 elements / Hahnium (element 105) / Chlorides / Relativistic effects

Summary

The retention behavior of volatile chlorides and oxychlorides of short-lived isotopes of group 5 elements Nb and 105 (Ha = hahnium) in quartz columns was studied using on-line isothermal gas chromatography. The 15-s ^{99g}Nb was produced from a ^{235}U-fission target at a reactor neutron beam line and 34-s ^{262}Ha in fusion reactions of ^{18}O + ^{249}Bk. The reaction products were continuously and rapidly transported to the chromatography apparatus with a carbon aerosol gas-jet system using He as carrier gas. Volatile chloride molecules were formed in a 900 °C reaction oven by adding HCl as reactive gas. Depending on trace amounts of O_2 in the system, either the pentachlorides or the oxytrichlorides, or a mixture thereof, were formed. The isotopes ^{99g}Nb and ^{262}Ha were unambiguously identified after gas chromatographic separation by measuring the characteristic γ-lines of ^{99g}Nb and by registering ^{262}Ha-^{258}Lr mother-daughter α-α correlations as well as spontaneous fission decays, respectively. The adsorption enthalpies of the investigated species on quartz surfaces were determined by analyzing the measured retention curves with a Monte Carlo model. Using an empirical correlation, the adsorption enthalpies were converted to sublimation enthalpies. The sublimation enthalpies of 95 ± 16 kJ · mol^{-1} and 124 ± 16 kJ · mol^{-1} determined for $NbCl_5$ and $NbOCl_3$, respectively, were in good agreement with literature data. In experiments with Ha-chlorides a yield curve with two components was observed. Sublimation enthalpies of ≤ 120 kJ · mol^{-1} and 152 ± 18 kJ · mol^{-1} were estimated for $HaCl_5$ and $HaOCl_3$, respectively. The estimated sublimation enthalpies were compared with theoretical predictions from relativistic calculations and with empirical extrapolations of chemical properties. In agreement with empirical extrapolations, a lower volatility was found for $HaOCl_3$ than for $NbOCl_3$.

1. Introduction

The investigation of the chemical properties of the elements at the end of the actinide and beginning of the transactinide series has challenged both theoretical and experimental chemists. The heaviest element whose chemical properties have been studied using radiochemical techniques is element 105 (Ha = hahnium)[1]. The reason for this special interest lies in the fact that near the end of the periodic table relativistic effects play an important role in determining the chemical properties of the heaviest elements. Recent calculations including the influence of relativistic effects allow now detailed predictions of the chemical properties of transactinide elements and their compounds.

Deviations from the regularities of the periodic system of the elements due to relativistic alterations of the electronic structures have been predicted for some time. Based on extrapolations from relativistic calculations for Lr [1, 2], Keller [3] suggested that in the case of Ha the ground state configuration could be [Rn]5 f^{14}6 d7 $s^2$7 $p^2_{1/2}$ rather than 6 $d^3$7 s^2, analogous to the 5 $d^3$6 s^2 configuration of its lighter homologue Ta. Therefore, Ha might be expected to behave similarly to Lu. However, chemical studies of Lr, Rf and Ha in both aqueous and gas phases (see Refs. [4–12] for recent review articles) clearly indicate, that the actinide series ends at Lr and the new 6 d transition series (the transactinide series) begins with Rf. It appears as if the changes in the chemical behavior of the first transactinides due to relativistic effects are less dramatic than previously anticipated. Therefore, very sophisticated relativistic calculations and unique chemical experiments have to be carried out to evaluate the influence of relativistic effects. Recently, Pershina *et al.* [13–16] published detailed predictions of the physicochemical properties of Ha halides. They anticipated that $HaCl_5$ and $HaBr_5$ should be more volatile than their lighter homologues.

[1] In this article the element names endorsed by the Nomenclature Committee of the American Chemical Society for use in the US are employed. By the choice of the element names in this article no prejudice about the priority of discovery is intended.

In contrast to these predictions, Ha-bromide was found to be appreciably less volatile than $NbBr_5$ or $TaBr_5$ [17]. Since the chemical composition of the separated single molecules of Ha-bromide could not be determined, the formation of $HaOBr_3$ was also considered. In our work the volatility studies were extended, and the retention behavior of Ha-chloride on quartz surfaces was investigated.

2. Halides of the group 5 elements Nb, Ta, Ha

2.1 Predicted chemical properties of Ha-halides and oxyhalides

In order to ascertain whether relativistic effects modify the chemical properties of Ha and its compounds compared to its lighter homologues, the expected chemical behavior must be predicted. On the one hand, sophisticated relativistic calculations lead to detailed predictions of physicochemical properties, on the other hand, also careful empirical extrapolations of periodic trends are invaluable, since these predictions account for relativistic alterations only in so far as these are already present in the lighter homologues. A comparison of the extrapolated physicochemical properties with the relativistic predictions can be regarded as an indicator for the influence of relativistic effects. In the following, the predicted relativistic and from periodic trends extrapolated properties of Ha-chlorides and oxychlorides will be discussed.

Using multiconfiguration Dirac-Fock (MCDF) calculations, Fricke *et al.* [18] calculated the electronic ground states for the group 5 elements V, Nb, Ta, and Ha in the charge states 0 to +5. In contrast to the calculated ground states for elements Lr ($7s^2 7p$) and Rf ($6d\,7s^2 7p$), a $J = 3/2^+$ $6d^3 7s^2$ (87.1%) configuration resulted for the atomic ground state of Ha. However, the calculated MCDF ground states for Ha, Ha^+, Ha^{+2}, and Ha^{+3} differ from the respective ground states of other group 5 elements. They have more s and $p_{1/2}$ character due to relativistic effects. Fricke *et al.* [18] also calculated values for the first five ionization potentials of all group 5 elements and ionic radii for the +2, +3, +4, and +5 ions of Ha.

Recently, the basic thermodynamic functions, the entropy, free energy, and enthalpy for Ha in electronic configurations d^3s^2, d^3sp, and d^4s^1 and for its +5 ionized state have been calculated as a function of temperature [19]. The calculations were based on the results of the calculations of the corresponding electronic states using the MCDF method.

Very detailed predictions of the chemical properties of Ha and its compounds, especially the halides and oxyhalides, were published by Pershina *et al.* [13–16]. They studied the chemical bonding in group 5 pentachlorides, pentabromides, and oxyhalides. By performing a number of relativistic molecular calculations for different geometries and molecular bond distances they arrived at the degree of ionic or covalent character of the metal-halide or metal-oxide bond. Their calculations showed that the compounds are predominantly covalent, however, the covalency does not change smoothly from Nb to Ta to Ha. There is a pronounced increase from Nb to Ta, while in $HaCl_5$ the bond is only slightly more covalent than in $TaCl_5$. The ionic character is almost equal for $NbCl_5$ and $TaCl_5$ whereas $HaCl_5$ is less ionic. From these data, the chemical bond strength in $HaCl_5$ was evaluated [13]. Compared to the pentachlorides of the group 5 elements, the pentabromides, show even higher covalency [14]. The low effective charge of Ha in $HaCl_5$ and $HaBr_5$ and its high covalency indicate that $HaCl_5$ and $HaBr_5$ should be more volatile than their lighter homologues. This trend should also be valid for the group 4 halides.

Since in macrochemistry the formation of pentahalides is often accompanied by the formation of oxyhalides, depending on temperature and oxygen concentration, the electronic structures of the group 5 oxyhalides were also calculated [15]. The calculations showed that Ha is an analog of the Nb and Ta oxyhalides; there is a steady decrease in effective charges from V to Ha, an increase in the covalent part of the binding energy, and an increase in molecular ionization potentials. The oxyhalides of group 5 elements are generally less volatile than the pure halides. No conclusion was reached for the periodic trends in volatility of the oxyhalides, since some of the constituents of the intermolecular interaction are counteracting and thus may cancel some of the differences in volatility expected for the pure pentahalides.

The classical predictions of the chemical properties of an unknown element exploit the fundamental relationships of the physicochemical data of the elements within the groups and the periods of the periodic table. In employing these periodic trends, the standard sublimation enthalpies ($\Delta H_s^{0(298)}$) of $HaCl_5$ and $HaOCl_3$ were extrapolated [20].

The physicochemical data for $NbCl_5$, $TaCl_5$, $NbOCl_3$, and $TaOCl_3$, along with the predicted relativistic and, from periodic trends, extrapolated values for $HaCl_5$ and $HaOCl_3$, are shown in Table 1. In Fig. 1 the vapor pressure curves for group 5 chlorides and oxychlorides are shown. In analogy to the procedure described in [14], the relativistic prediction of the vapor pressure curve of $HaCl_5$ employed the calculated, effective charges on the ligands from [13]. Even though the errors on the experimentally determined vapor pressure curves are considerable, and very large on the predicted vapor pressure curves for $HaCl_5$ and $HaOCl_3$, the relative volatility can be regarded as a reasonable basis for the interpretation of the experimental results on the volatility of Ha chlorides. If the extrapolated vapor pressure curves are correct, $HaCl_5$ should exhibit a similar volatility compared to $NbCl_5$ and $TaCl_5$, whereas $HaOCl_3$ should be less volatile than $NbOCl_3$ or $TaOCl_3$. Compared to the extrapolated vapor pressure curve for $HaCl_5$, the relativistic calculations predict a $HaCl_5$ which is volatile at a 50°C lower temperature than the homologous compounds.

Table 1. Physicochemical properties of $NbCl_5$, $TaCl_5$, $NbOCl_3$, and $TaOCl_3$ along with the predicted relativistic- and from periodic trends extrapolated values for $HaCl_5$ and $HaOCl_3$

Molecule	T_m[a]	T_b[b]	$\Delta H_s^{0(298)}$[c]	$\Delta S_s^{0(298)}$[d]	$\log p = A + B \cdot T^{-1}$[e] (torr)		Temperature range	Reference
	(K)	(K)	(kJ · mol^{-1})	(J · mol^{-1} · K^{-1})	A	B	(K)	
$NbCl_5$	479	519	94.0	190.1	12.81	−4911	298−479	[21]
$TaCl_5$	490	506	94.1	191.2	12.87	−4917	298−490	[21]
$HaCl_5$			94.2	192.1	12.91	−4921		this work
			85			−4446		calc. [13, 14]
$NbOCl_3$		607	128.5	216.3	14.18	−6712	298−607	[21]
$TaOCl_3$		600[f]	170.1	222.3	14.50	−8887	298−600	[21]
$HaOCl_3$			180.0	226.5	14.71	−9403		this work

[a] T_m: melting point.
[b] T_b: boiling point.
[c] $\Delta H_s^{0(298)}$: standard sublimation enthalpy at 298 K.
[d] $\Delta S_s^{0(298)}$: standard sublimation entropy at 298 K.
[e] p: vapor pressure.
[f] Decomposition temperature.

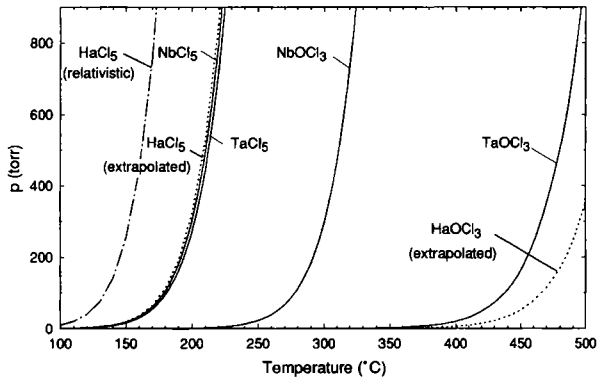

Fig. 1. Vapor pressure curves for Nb and Ta pentachlorides and oxytrichlorides from Ref. [21], along with the predicted, relativistic vapor pressure curve for $HaCl_5$ (dash-dotted line) calc. from [16], and, from periodic trends extrapolated vapor pressure curves for $HaCl_5$ and $HaOCl_3$ (dotted lines).

2.2 Previous experiments on the volatility of Ha-halides

First gas chemistry experiments with the isotope ^{261}Ha were performed by Zvara *et al.* [22, 23] using thermochromatography. They observed that Ha forms a more volatile chloride than $HfCl_4$ (and $RfCl_4$) but less volatile than $NbCl_5$. In a second experiment, the thermochromatographic behavior of $HaBr_5$ was studied in Ni columns [24]. Fission tracks were observed at higher temperatures than the deposition zone of $NbBr_5$. After correcting for the different half-lives of ^{261}Ha and ^{90m}Nb, the authors concluded that $HaBr_5$ is less volatile than $NbBr_5$ and $TaBr_5$ (which is similar in volatility to $NbBr_5$). They found that the volatility of $HaBr_5$ was close to that of $HfBr_4$. Recently, Zvara *et al.* [25] repeated their experiments on the volatility of group 5 chlorides and bromides now using the longer lived isotopes ^{262,263}Ha. Even though they registered orders of magnitude more spontaneous fission (SF) decays than in their previous experiments, the background of ^{256}Fm (92% SF) was a serious handicap. Nevertheless, the results seemed to confirm the data from earlier experiments. A major draw-back of all thermochromatography experiments is the fact that only SF-tracks left in the chromatography column can be observed, which prevents positive identification of the nuclide by the detection of α particles (and thus $\alpha-\alpha$ correlations) or even the determination of the half-life of the observed SF-activity.

A series of experiments to study the volatility of group 5 bromides employing the OLGA technique [26, 27] (**O**n-Line **G**as-chemistry **A**pparatus) were described by Gäggeler *et al.* [17, 28]. The decay of the nuclides ^{262,263}Ha was detected after chemical separation at the exit of the chromatography column. The observed trend in volatility was Nb ≈ Ta > Ha [17]. Only preliminary results on the volatility of group 5 chlorides are available [29, 30]. A detailed overview of OLGA experiments with group 5 halides is given in Ref. [12].

3. Experimental

3.1 Production and transport of ^{262,263}Ha and ^{99g}Nb

The nuclides ^{262,263}Ha were produced in the ^{249}Bk(^{18}O, 4,5 n) reaction at the LBL 88-Inch Cyclotron using the target arrangement shown in Ref. [7]. The beam of 117 MeV ^{18}O ions, collimated by a graphite ring, passed through a HAVAR™ vacuum isolation window, a volume of nitrogen cooling gas, and the Be target backing before interacting with the target material. The target, containing 790 μg · cm^{-2} of ^{249}Bk was prepared by stepwise electrodeposition of $Bk(NO_3)_3$ from isopropanol solution on a 2.4 mg · cm^{-2} Be foil in a 6-mm diameter spot. Each deposited layer was converted to the oxide by heating to 500°C for at least 20 min. The ^{249}Bk was prepared on September 4, 1993, and the experiment conducted 4 weeks later. Hence, about 7% of the 320-d ^{249}Bk had already decayed into

^{249}Cf. The calculated beam energy in the Bk target was 98–99 MeV. Typical beam currents of $^{18}O^{5+}$ used throughout the experiments were 0.5 pμA ($\cong 3 \cdot 10^{12}$ particles $\cdot s^{-1}$).

Studies with 15-s ^{99g}Nb were carried out at the PSI SAPHIR reactor, Switzerland. A 180 $\mu g \cdot cm^{-2}$ ^{235}U target electrodeposited on a 4.05 $mg \cdot cm^{-2}$ aluminum foil was bombarded with $4.6 \pm 0.5 \times 10^6$ thermal neutrons $\cdot s^{-1} \cdot cm^{-2}$ over a beam spot of 50 mm diameter [26].

In both systems the reaction products recoiling out of the target material were thermalized in He loaded with carbon aerosols and transported through a polyethylene capillary to the chromatography apparatus with a He flow rate of 1 $l \cdot min^{-1}$. The carbon aerosols were produced using a spark discharge generator consisting of a capacitor and two cylindrical carbon electrodes of 3 mm diameter, similar to the set-up described in [31]. The generator was initially developed to operate with N_2 or Ar as carrier gas. However, due to the high ionization potential of He a self confining plasma channel did not form, and no constant and sufficient evaporation of the electrode material could be achieved. This problem was solved using an approach by Stober [32]. The bottom electrode was surrounded by a brass cone and negatively charged by a high voltage power supply. The breakdown voltage in our set-up reached about 1 kV. This way, the electric field geometrically confined the plasma channel and a constant evaporation of the electrode material was achieved. The generated, electrically charged aerosols were neutralized with a 2 mCi ^{85}Kr source. The mean mobility equivalent diameter of the particles was about 200–300 nm, measured with a differential mobility analyzer [33].

3.2 Separation principle (OLGA technique)

A new version of the isothermal chromatography system, OLGA III [34], was used to study the volatility of the produced molecules. The basic design of the OLGA method described in Refs. [26, 27] was improved in several important areas. An all quartz design was chosen to improve cleanliness and to prevent corrosion. The column length was increased to 1.9 m and mechanical stability was achieved by winding the capillary (1 mm i.d.) around a quartz rod of 10 mm diameter. The column was placed inside a commercial gas chromatography oven (Carlo Erba Instruments, HRGC 5160, Mega Series) which provided excellent temperature stability up to a maximum temperature of 500°C. The recluster unit was also redesigned. By turbulently mixing the separated species with a KCl aerosol (N_2/KCl or Ar/KCl), in a 15 cm^3 volume, an efficient and stable attachment of the volatile compounds to the particles was achieved. Assuming a typical gas flow of 2.5 $l \cdot min^{-1}$, the residence time in the recluster unit was reduced from about 20 s [26] to about 2 s. Using a cooled recluster chamber has two advantages: the heat brought into the chamber by the carrier gas from the chromatography can be very efficiently removed and the gas 'layer' on the wall of the recluster vessel is cold, thus reducing losses by diffusion to the walls of the recluster vessel. For a schematic of the experimental set-up we refer to Ref. [12]. The chromatography column was subdivided into two sections. In the first section the reaction products, attached to carbon aerosol particles, were stopped on a quartz wool plug. This section was kept at a fixed temperature of 900°C. At the position of the quartz wool plug, HCl was added at a flow rate of about 100–200 $ml \cdot min^{-1}$. The second part of the quartz column served as the isothermal chromatography-section. In different experiments the temperature was varied between 100°C and 350°C. Volatile chloride species, formed at the position of the quartz wool plug, were then transported along the cooler chromatography section of the column by the carrier gas. Here the molecules interacted with the column surface in numerous sorption/desorption steps, with retention times indicative of their volatility. Volatile products leaving the column were reattached to new aerosol particles in the recluster chamber for transport to the detection system.

3.3 MG-RAGS detection and data acquisition system

The detection system consisted of the MG (**M**erry-**G**o-round) rotating wheel system [35]. In the MG system, the aerosols carrying the separated activities were deposited on thin polypropylene foils (30–40 $\mu g \cdot cm^{-2}$) around the periphery of an 80 position wheel. Each 30 s the wheel was stepped to move the collected activity successively between pairs of PIPS (**P**assivated **I**mplanted **P**lanar **S**ilicon) detectors. This new detector type is chemically inert. Six pairs of PIPS detectors registered α-particles and SF-events which were recorded in an event-by-event mode. Each wheel was used for two revolutions. The MG chamber was evacuated with an inert vacuum pump; the pump exhaust gases, still containing the reactive agents, were neutralized in a NaOH scrubber system. The MG wheel system allowed the registration of α events from both sides of the deposition spot, as well as the detection of single and coincident SF-events with a detector efficiency of about 60% [36].

In experiments with short-lived isotopes of Nb, the aerosols carrying the separated activities were retained on glass fiber filters and measured in front of a high purity Ge detector. The glass fiber filter was replaced before each measurement.

4. Results and discussion

4.1 Experiments with Nb-chlorides

Even under strong chlorinating conditions, Nb has a tendency to form not only the volatile $NbCl_5$, but also

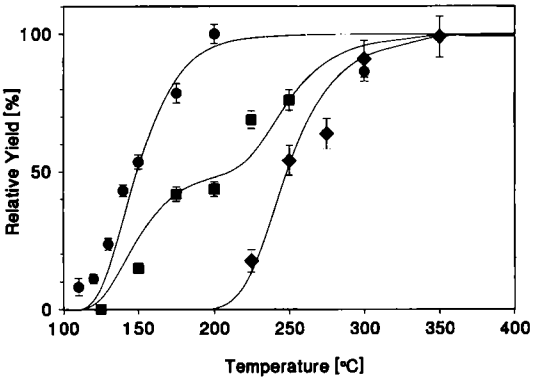

Fig. 2. Relative yields of 15-s ^{99g}Nb-pentachloride and oxytrichloride as a function of isothermal temperature and O_2 concentration (● $^{99g}NbCl_5$, $p(O_2) \leq 1$ ppmv, $-\Delta H_a^{0(T)}(NbCl_5) = 80$ kJ · mol^{-1}; ■ 50% $^{99g}NbCl_5$ + 50% $^{99g}NbOCl_3$, 1 ppmv $\leq p(O_2) \leq 80$ ppmv; ◆ $^{99g}NbOCl_3$, $p(O_2) \geq 80$ ppmv, $-\Delta H_a^{0(T)}(NbOCl_3) = 99$ kJ · mol^{-1}). The solid lines were calculated with a Monte Carlo model using the $\Delta H_a^{0(T)}$-values which best fit the measured data.

the less volatile $NbOCl_3$ or the only slightly or non-volatile NbO_2Cl or NbO_2, respectively. Obviously, the concentration of O_2 and oxygen containing compounds (e.g. H_2O) is critical in volatility experiments with group 5 element chlorides and needs to be carefully monitored. In a first step, the quality of the He carrier gas, the diffusion of O_2 through the walls of the 130 m long polyethylene transport capillary, and the leakage of the system was measured. The free O_2 partial pressure was measured using a solid electrolyte cell. The O_2 content of the He carrier gas in the tank was about 1 ppmv. After the 130 m long capillary between the SAPHIR reactor and our chemistry laboratory, a much higher O_2 content of 80 ppmv was measured at a flow rate of 1 l · min^{-1}. Contributions from other sources of O_2 that could not be measured were impurities in the reactive gases (HCl) and the quartz surface of the chromatography column. The chemical yields measured for 15-s ^{99g}Nb are shown as a function of the isothermal temperature and the O_2 concentration in Fig. 2. The maximum yields of every experiment were normalized to 100%. The carrier gas flow was 1 l · min^{-1} He loaded with C aerosol particles; 200 ml · min^{-1} HCl were added as reactive gas. The recluster gas flow was 1.75 l · min^{-1} N_2, loaded with CsCl aerosol particles. With HCl (99.8%) as reactive gas only one species was formed, which, based on its volatility, was later identified as $NbOCl_3$. When the HCl was purified with activated charcoal at 1000 °C, two species of different volatility were observed. Both species were produced in about equal ratios, which resulted in a yield curve with two steps, consisting most likely of about 50% $NbCl_5$ and 50% $NbOCl_3$. When, in addition, stripes of graphite paper, that were first dipped into $SOCl_2$, were introduced into the 900 °C reaction section of the chromatography column, only the more volatile species was observed. Under these conditions $NbCl_5$ was formed. By purifying the reactive gases, as well as the carrier gas from traces of O_2, a concentration of about 1 ppmv or less was reached.

The data were analyzed using a novel approach for determining the adsorption enthalpies ($\Delta H_a^{0(T)}$) of the investigated species. On the basis of a microscopic model of gas-solid thermochromatography in open columns proposed by Zvara [37], a Monte Carlo code was developed [38], which calculated the expected yield of a chemical species for a given $\Delta H_a^{0(T)}$-value at each measured isothermal temperature. This model is well suited to accommodate the influence of the high carrier gas flow rates, the actual temperature profiles in the column, and to account for the different half-lives of the investigated species. For each isothermal temperature the interaction with and the transport through the column, for each of a large number of sample molecules ($\geq 10^4$), was modeled. This calculation resulted in a curve of yield versus isothermal temperature for each value of $\Delta H_a^{0(T)}$. The curve for the $\Delta H_a^{0(T)}$-value which fit the measured data was chosen by a least squares method. The shapes of the calculated yield curves reproduce the measured yield curves very well (Fig. 2). The resulting adsorption enthalpies were $\Delta H_a^{0(T)}(NbCl_5) = -80 \pm 1$ kJ · mol^{-1} and $\Delta H_a^{0(T)}(NbOCl_3) = -99 \pm 1$ kJ · mol^{-1}. The error limits (1 σ) do not include systematic errors. In Table 2, a compilation of experimental $\Delta H_a^{0(T)}$-values from the literature, measured for carrier free amounts of $NbCl_5$ and $NbOCl_3$ on quartz surfaces, along with the results from this work, are shown. Values between −66 kJ · mol^{-1} and −88 kJ · mol^{-1} for $\Delta H_a^{0(T)}(NbCl_5)$ and between −74 kJ · mol^{-1} and −99 kJ · mol^{-1} for $\Delta H_a^{0(T)}(NbOCl_3)$ were reported, respectively. The large spread of the data of 22 kJ · mol^{-1} and 25 kJ · mol^{-1} for $\Delta H_a^{0(T)}(NbCl_5)$ and $\Delta H_a^{0(T)}(NbOCl_3)$, respectively, is probably due to different analysis procedures and also depends on the selected standard state. It is, therefore, impossible to evaluate the quality of our data solely by comparison with literature data. In our calculations, the adsorption residence time is governed by the Frenkel equation. The recommended value for τ_0 (period of oscillations of the molecule in the adsorbed state perpendicular to the surface) for quartz surfaces is $2 \cdot 10^{-13}$ s [39].

Eichler *et al.* [40] have established a linear correlation between $\Delta H_a^{0(T)}$ of chlorides on quartz surfaces and $\Delta H_s^{0(298)}$, the standard sublimation enthalpy:

$$\Delta H_a^{0(T)} = -(0.655 \pm 0.042) \cdot \Delta H_s^{0(298)} - (18.0 \pm 8.8) \quad [\text{kJ} \cdot \text{mol}^{-1}] \qquad (1)$$

Using this correlation and $\Delta H_s^{0(298)}$-values from [21], $\Delta H_a^{0(T)}(NbCl_5) = -79.6 \pm 9.6$ kJ · mol^{-1} and $\Delta H_a^{0(T)}(NbOCl_3) = -102.2 \pm 10.3$ kJ · mol^{-1} were calculated, in good agreement with the data from this work.

4.2 Experiments with ^{262,263}Ha

4.2.1 Nuclear decay properties of ^{262}Ha and ^{263}Ha

At a 99 MeV beam energy in the target both isotopes ^{263}Ha and ^{262}Ha are formed in the ^{249}Bk(^{18}O, 4,5n) re-

Table 2. Experimentally determined adsorption enthalpies ($-\Delta H_a^{0(T)}$) on quartz surfaces of $NbCl_5$ and $NbOCl_3$ from this work and from literature data

$-\Delta H_a^{0(T)}(NbCl_5)$ (kJ · mol^{-1})	Chlorinating agent	$-\Delta H_a^{0(T)}(NbOCl_3)$ (kJ · mol^{-1})	Chlorinating agent	Reference
−88±4	Cl_2/CCl_4	−98	$SOCl_2$	[40]
−68±3	not available	−99±10	CCl_4	[41, 42]
−69±3	CCl_4	−96±3	CCl_4/H_2O	[43]
−67±7	CCl_4			[44]
−66±2	$SOCl_2$	−74±2	$SOCl_2/O_2$	[45]
−70±5	Cl_2/CCl_4			[29]
−86	$SOCl_2$	−99	$SOCl_2/O_2$	[46]
−80±1	HCl(purified)	−99±1	HCl(99.8%)	[this work]

Table 3. Decay properties of ^{262}Ha observed in various $^{18}O + ^{249}Bk$ experiments (depending on the beam energy, the half-lives for ^{262}Ha may vary due to varying contributions of ^{263}Ha)

Beam energy	α-energies, or range of α-energies		No. of events	Type of events	$T_{1/2}$ ^{262}Ha	$T_{1/2}$ ^{258}Lr	Branching ratio (EC or SF)	Reference
(MeV)	^{262}Ha	^{258}Lr			(s)	(s)	(%)	
			35	α−α	43±15	5±2		
92−97	8.45, 8.66	8.61	~200	α-single	40±10	4.5±2	60	[48]
			~300	SF-single	25±10			
	8.45(75%)							
100	8.53(16%)			α-single	34.1±4.6		78±6	[53, 54]
	8.67 (9%)		~180	SF-single	32.6±6.5			
99	not measured			SF-single	$35.2^{+10.4}_{-7.2}$			[55]
			5	α−α	22^{+17}_{-8}	$2.5^{+1.9}_{-1.0}$		
101	8.44−8.68	8.60−8.75	21	α-single	28^{+7}_{-5}		49±13	[49]
			26	SF-single	32^{+8}_{-6}			
			14	α−α	$35.3^{+12.3}_{-7.2}$	$5.5^{+2.0}_{-1.2}$		
98−99	8.34−8.69	8.52−8.66	30	α-single	$39.8^{+8.9}_{-6.2}$		51±11	[50]
			96	SF-single	33.5±9.4			
98−99	not analyzed			SF-single	44^{+19}_{-12}			[17]
			8	α−α	$32.0^{+10.2}_{-7.7}$	$4.2^{+1.5}_{-1.1}$		
99	8.43−8.67	8.54−8.68	39	α-single	$35.7^{+6.9}_{-5.4}$		33	[47]
			23	SF-single	$31.4^{+6.0}_{-5.0}$			
99	8.40−8.70	8.40−8.70	7	α−α	28^{+17}_{-8}	$3.8^{+2.3}_{-1.0}$		[8, 30]
			122	SF-single	47^{+11}_{-8}			
98−99	8.40−8.75	8.40−8.75	27	α−α	$22.0^{+4.3}_{-3.5}$	$6.8^{+2.2}_{-1.5}$	42±19	this work
			45	SF-coinc	$21.0^{+4.9}_{-4.5}$			

actions with cross sections of 2±1 nb and 6±3 nb, respectively [47]. The isotope ^{262}Ha was discovered by Ghiorso *et al.* [48] by observing α−α correlations originating from the α decay of ^{262}Ha followed shortly in time by the α decay of the ^{258}Lr daughter. This α−α correlation technique has been applied in subsequent chemical studies of this isotope [28, 30, 47, 49−51]. In Table 3 the decay properties of ^{262}Ha and ^{258}Lr observed in various experiments are summarized. For convenience, the results of this work are also included in the table. With the discovery of ^{263}Ha, the SF- or EC branch in ^{262}Ha decreased from about 50% to 33% [47]. ^{263}Ha has a half-life of 27^{+10}_{-7} s and decays by α emission (8.355 MeV, 43%) and by SF (57%) [52]. However, no ^{263}Ha−^{259}Lr α−α correlations, which would definitely confirm the assignment to ^{263}Ha, have been observed to date. Uncertainties in the actual beam energies may have lead to varying contributions of ^{263}Ha, which might explain some of the inconsistencies observed in the decay properties of ^{262}Ha.

In Fig. 3 the combined, energy calibrated spectra from all chemistry runs collected with 8245 samples are shown. The main activities were due to contaminants, namely 2.17-m ^{211}Bi (6.62 MeV, 6.28 MeV), 25.2-s ^{211m}Po (7.27 MeV), and 45.1-s ^{212m}Po (11.65 MeV, 9.08 MeV), presumably formed from Pb impurities in the ^{249}Bk target. Unfortunately, Po and Bi formed volatile chlorides and were thus not retained. Alpha particles from the ^{262}Ha-^{258}Lr decay sequence were expected in the energy range between 8.40 and

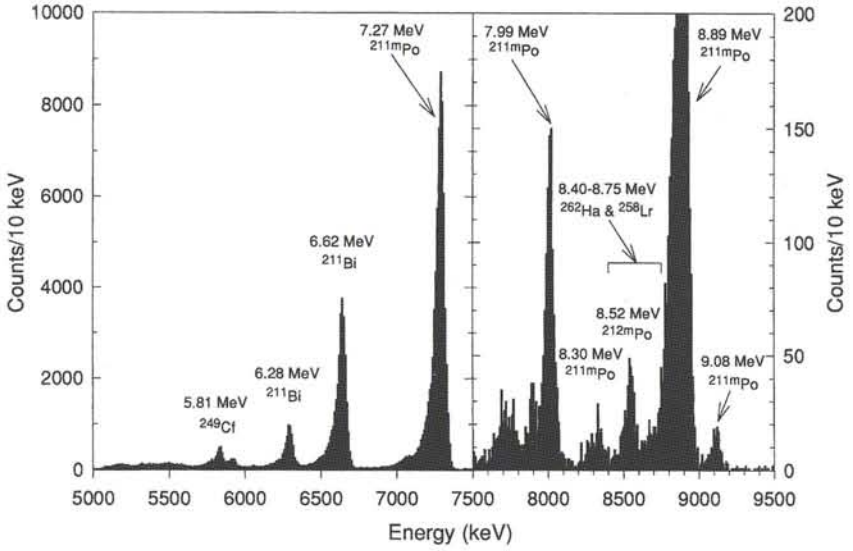

Fig. 3. Sum of the measured, energy calibrated α-spectra from detector pairs 1 through 5 (0−150 s) from all gas phase chromatography experiments. The vertical scale above 7.5 MeV was expanded.

8.75 MeV. This energy range also contained a weak α-line from ^{212m}Po (8.52 MeV, 2.05%). In addition, the tailing of the α-peak of ^{211m}Po (8.89 MeV, 7.04%) contributed to the count rate in the 8.40 and 8.75 MeV energy range. The combined spectra contained a total of 650 counts in the energy range 8.40 to 8.75 MeV. From the count rates of the main α-line of ^{212m}Po (11.65 MeV, 94%) 276±16 counts were attributed to ^{212m}Po contaminants. By fitting a Gaussian with an exponential tail function [56] to the ^{211m}Po peak at 8.89 MeV, the tailing into the 8.40 to 8.75 MeV area contributed 269±16 counts, which amounted to 5% of the total peak area. Under the assumption that no other contaminating activities were present in this energy range, 105±35 counts were due to ^{262}Ha and ^{258}Lr. The ingrowth of ^{258}Lr from the decay of ^{262}Ha started immediately after the chemical separation, whenever a ^{262}Ha nuclide left the chromatography column. With a 30 s collection interval on the MG wheel and an assumed mean reclustering time of 2 s, about 9% of the α-decaying ^{262}Ha decayed to ^{258}Lr at the beginning of the counting interval. The efficiency for detecting an α-particle from the source was 60% [36] for top plus bottom detector with an estimated error of 4%. From a source containing e.g. a mixture of 91 ^{262}Ha (decaying by α-decay) and 9 ^{258}Lr nuclides 109 α-particles (52 ^{262}Ha α-particles and 57 ^{258}Lr α-particles) will be registered within the counting interval of 150 s, assuming half-lives of 34.1 s for ^{262}Ha [53] and 3.92 s for ^{258}Lr [36], respectively. Thus, from the 105±35 counts assigned to ^{262}Ha and ^{258}Lr, 50±24 were ^{262}Ha α-particles (48%) and 55±25 (52%) were ^{258}Lr α-particles. In order to calculate the expected number of true $\alpha-\alpha$ correlations, a correlation time window of 20 s was chosen. The correlation time should be sufficiently long to allow almost all of the daughter nuclides to decay, but sufficiently short in order to keep the random correlation rate small. Taking into account that for mother α-particles that are registered after 130 s, the correlation time window gets shorter, the decay of the daughter nuclide occurs with a probability of 92%. With a detection probability of 60±4% for the daughter α-particles 28±13 true $\alpha-\alpha$ correlations should be observed. The error limits (1 σ) were calculated with the law of Gaussian error propagation and assuming Poisson statistics.

In order to assess the validity of the correlation method, the random correlation rate in the same energy- and time-correlation window was calculated. First, the number of nuclides present at the beginning of the 150 s counting interval decaying with an α-particle in the 8.40 to 8.75 MeV energy range, was calculated. These were ^{212m}Po 511±46 (48%), ^{211m}Po 456±41 (43%), ^{262}Ha 87±42 (8%), and ^{258}Lr 9±9 (1%). A total of 1063±76 nuclides were collected with 8245 samples (0.129±0.009 nuclides/sample). Assuming Poisson statistics, the number of samples containing 2 nuclides is $P(2, 0.129) = 60.2^{+8.3}_{-7.8}$. The possible combinations that could lead to observed random correlations and the corresponding probabilities are summarized in Table 4. The decay probability was calculated by integrating the product of the probabilities to find the first α-particle within a time interval from $t=0$ to 130 s and the second α-particle within a time interval from t to t + 20 s. The time window from t = 130 s to 150 s was integrated separately. There, the product of the probabilities to find the first α-particle within the interval from t = 130 to 150 s and to find the second α-particle within the interval from t = t to 150 s was integrated within the limits 130 and 150 s. From the sum of all possible combinations a total of $4.9^{+3.2}_{-2.2}$ random $\alpha-\alpha$ correlations was expected in the present experiment. Almost all of the random $\alpha-\alpha$ correlations originated from samples containing two Po nuclides. The most probable random $\alpha-\alpha$ correlation originated form the ^{211m}Po-^{211m}Po pair, fol-

Table 4. Possible combinations of two nuclides/sample and the expected number of detected random $\alpha-\alpha$ correlations within a correlation time window of 20 s

1. Nuclide		2. Nuclide		% of the samples	Number of samples	Detection probability	Decay probability	Random correlations
Mother α	Daughter α	Mother α	Daughter α					
^{211m}Po	–	^{211m}Po	–	18.36%	11.05	36.00%	42.29%	1.68
^{211m}Po	–	^{212m}Po	–	20.59%	12.39	36.00%	16.93%	0.76
^{211m}Po	–	^{262}Ha	(^{258}Lr)	3.55%	2.14	14.40%	19.19%	0.06
^{211m}Po		(^{262}Ha)	^{258}Lr			14.40%	19.98%	0.06
^{211m}Po	–	^{258}Lr	–	0.35%	0.21	36.00%	13.07%	0.01
^{212m}Po	–	^{211m}Po	–	20.59%	12.39	36.00%	15.13%	0.67
^{212m}Po	–	^{212m}Po	–	23.09%	13.90	36.00%	26.11%	1.31
^{212m}Po	–	^{262}Ha	(^{258}Lr)	3.98%	2.39	14.40%	14.29%	0.05
^{212m}Po		(^{262}Ha)	^{258}Lr			14.40%	15.13%	0.05
^{212m}Po	–	^{258}Lr	–	0.39%	0.24	36.00%	7.76%	0.01
^{262}Ha	(^{258}Lr)	^{211m}Po	–	3.55%	2.14	14.40%	17.96%	0.06
(^{262}Ha)	^{258}Lr	^{211m}Po	–			14.40%	15.54%	0.05
^{262}Ha	(^{258}Lr)	^{212m}Po	–	3.98%	2.39	14.40%	14.97%	0.05
(^{262}Ha)	^{258}Lr	^{212m}Po	–			14.40%	13.75%	0.05
^{262}Ha	(^{258}Lr)	^{262}Ha	(^{258}Lr)	0.69%	0.41	5.76%	33.29%	0.01
^{262}Ha	(^{258}Lr)	(^{262}Ha)	^{258}Lr			5.76%	17.51%	0.00
(^{262}Ha)	^{258}Lr	^{262}Ha	(^{258}Lr)			5.76%	14.92%	0.00
(^{262}Ha)	^{258}Lr	(^{262}Ha)	^{258}Lr			5.76%	32.41%	0.01
^{262}Ha	(^{258}Lr)	^{258}Lr	–	0.07%	0.04	14.40%	10.01%	0.00
(^{262}Ha)	^{258}Lr	^{258}Lr	–			14.40%	5.01%	0.00
^{258}Lr	–	^{211m}Po	–	0.35%	0.21	36.00%	36.62%	0.03
^{258}Lr	–	^{212m}Po	–	0.39%	0.24	36.00%	24.35%	0.02
^{258}Lr	–	^{262}Ha	(^{258}Lr)	0.07%	0.04	14.40%	29.96%	0.00
^{258}Lr	–	(^{262}Ha)	^{258}Lr			14.40%	27.55%	0.00
^{258}Lr	–	^{258}Lr	–	0.01%	0.00	36.00%	97.09%	0.00
Total				100.00%	60.18			4.94

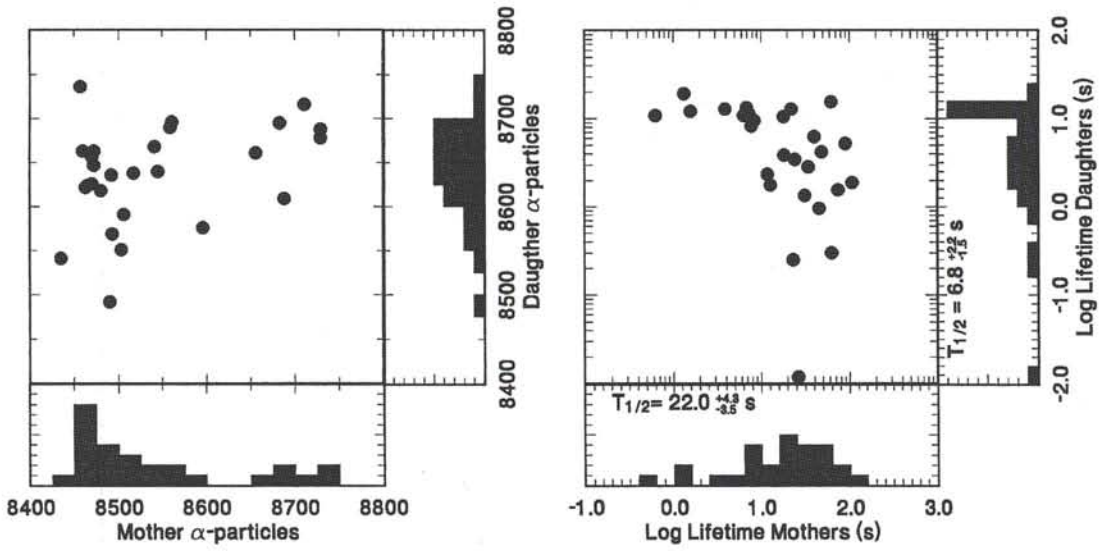

Fig. 4. Energy- and decay time correlation diagrams for $\alpha-\alpha$ correlations in the energy window 8.40–8.75 MeV for mother and daughter α-particles and a correlation time of 20 s.

lowed by the ^{212m}Po-^{212m}Po pair. Since the number of random correlations depended on the number of the registered Po α-particles in the 8.40 to 8.75 MeV energy range and thus depended on the temperature of the column, the above calculations had to be corrected slightly. If the random correlation rate was calculated separately for each temperature, the number of random correlations slightly increased to $5.5^{+3.3}_{-2.3}$.

The data analysis revealed 27 $\alpha-\alpha$ correlations, compared to 33 ± 14 expected correlations (28 true and 5.5 random). In Fig. 4 the energy- and the decay time correlation diagrams from the observed 27 correlations

are shown. The mean life times yield half-lives of $22.0^{+4.3}_{-3.5}$ s for the mother- and $6.8^{+2.2}_{-1.5}$ s for the daughter nuclide. The decay curve analysis was performed by a single component maximum likelihood decay curve fit [57] to the recorded life times. The daughter half-life is slightly longer than the literature value of $3.92^{+0.35}_{-0.31}$ s [36], while the mother half-life is somewhat shorter than the $34.1^{+4.6}_{-4.6}$ s literature value [53]. The probability to observe a half-life of the mother within the error limits of $22.0^{+4.3}_{-3.5}$ s from 27 measured life times is about 20%, compared to 68% to observe a half-life within the error limits of the literature value (provided that the literature value is correct). Similarly, the probability to observe a daughter half-life within the error limits of $6.8^{+2.2}_{-1.5}$ s is also about 20%. Nevertheless, the relatively long daughter half-life may be an indication that even with restrictive energy criteria, not all random contributions can be removed.

Along with the α-particles, SF-events were registered as well. A total of 54 coincident (simultaneous detection of both fragments in the top- and the bottom detector) SF-events were registered. It is not clear whether ^{262}Ha and/or ^{263}Ha is the fissioning nuclide or if SF occurs after EC-decay to ^{262}Rf, or after α or EC-decay of ^{263}Ha. Since detector pair No. 6 was located in position 12 of the MG wheel system, measuring decays in the time interval from 330 to 360 s, the contribution of a ^{256}Fm contamination could be determined with better accuracy than in earlier experiments. ^{256}Fm was formed either directly by a nucleon transfer reaction mechanism and/or by EC-decay of ^{256}Md, with cross sections on the order of few 100 nb [58]. Obviously the decontamination from actinides was not sufficient to suppress the unwanted SF-activity completely. A maximum likelihood decay curve fit [57] to the recorded life times, assuming a minor ^{256}Fm contamination yielded a half-life for ^{262,263}Ha of $21.0^{+4.9}_{-4.5}$ s and a ^{256}Fm contribution of 16%. The SF half-life is in agreement with the half-life determined from the $\alpha-\alpha$ correlation analysis, but again short compared to the literature values of $32.6^{+6.5}_{-6.5}$ s for ^{262}Ha [53] or 27^{+10}_{-7} s for ^{263}Ha [52].

4.2.2 *Chemical properties of Ha-chlorides*

The conditions at which the experiments where conducted were as close as possible to the conditions where $NbCl_5$ was separated in the test experiments. The carrier gas flow rate was 0.7 to 1 l · min^{-1} He loaded with C-aerosols. As chlorinating agent HCl, purified with activated charcoal at 900°C at a flow rate of 100 to 200 ml · min^{-1}, was added. In front of the quartz wool plug, stripes of graphite paper, that were first dipped into $SOCl_2$, were introduced. The reaction oven was heated to 950°C. As recluster gas 1 to 1.5 l · min^{-1} Ar loaded with KCl aerosols was used. The yield curve of Ha can be constructed on the basis of the registered $\alpha-\alpha$ correlations and on the basis of the observed SF-events for each isothermal temperature. A calculated random correlation rate was subtracted from the observed number of $\alpha-\alpha$ correlations according to a procedure described in the previous section. These corrections were always <30%. The resulting $\alpha-\alpha$ correlation detection rates were normalized to the beam integral and to the yield observed at 350°C. The absolute chemical yield for Ha could not be determined, since without chemical separation Ha cannot be identified. The yield of the 25.2 s ^{211m}Po contaminant in the chemistry runs was 35% to 40% at 350°C compared to the activity collected directly with the aerosol gas jet on the MG-wheel. The yield curve for $\alpha-\alpha$ correlations and ^{211m}Po is shown in Fig. 5a. The errors on the data points encompass 68% of the probability in a Poisson distribution. At 350°C about twice as many correlations were observed than at 300°C and at lower temperatures. Even at 200°C one $\alpha-\alpha$ correlation was observed. The calculated random correlation rate at this temperature was 0.02 correlations. It appears as if the yield curve for Ha-chlorides consisted of two species, one of which is volatile at temperatures ≤200°C, whereas the second one becomes volatile at >300°C. This behavior should also be observed for the chemical yields of SF-events. In order to correct for the 16% ^{256}Fm contamination of the SF-data, all the runs were analyzed for α-particles of ^{252}Fm through ^{255}Fm. The Fm contamination at all measured temperatures normalized to the beam integral was about constant. Thus, the SF-yields were corrected accordingly and normalized to the beam integral. The normalized SF-yields are shown in Fig. 5b. A similar picture as observed for the $\alpha-\alpha$ correlations emerged. The SF-yields at 350°C are significantly higher than at 300°C and lower temperatures. But the

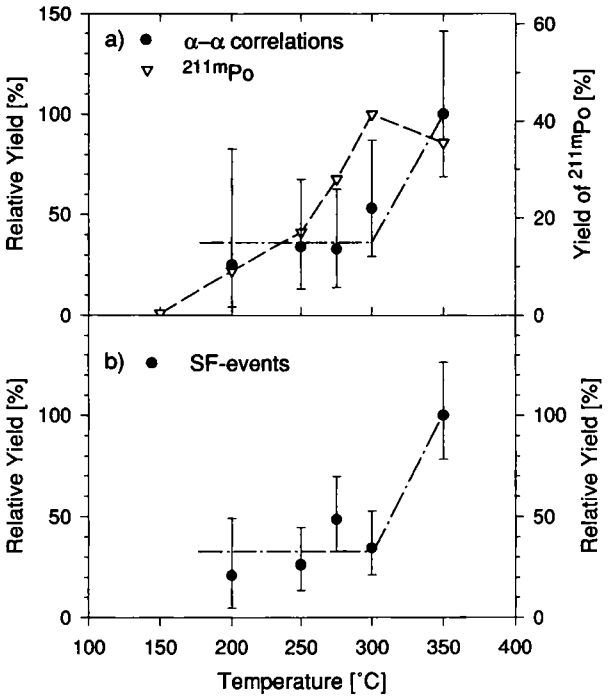

Fig. 5. Relative yields observed for a) $\alpha-\alpha$ correlations (8.40–8.75 MeV, $t_{corr.}$ = 20 s) and ^{211m}Po, and, b) SF-events (detector pairs 1–5) shown as a function of isothermal temperature.

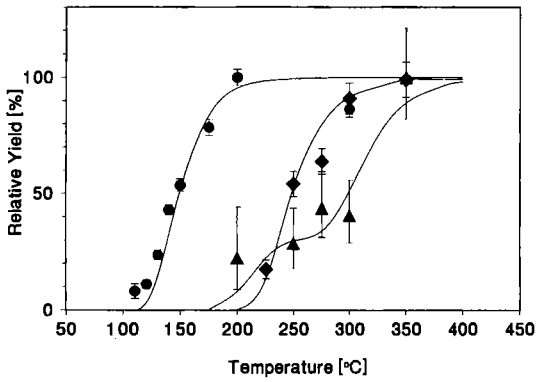

Fig. 6. The combined yield curves for Ha-chlorides consisting of both $\alpha-\alpha$ correlation and SF-yields (from Fig. 5) along with the data measured for $NbCl_5$ and $NbOCl_3$ (from Fig. 2) are shown as a function of isothermal temperature. The yield curves were analyzed with the Monte Carlo model (solid lines).

yields remain constant, down to the lowest measured temperature of 200 °C and are not dropping to zero as would be expected if only one chemical species were present. Since the SF-yields reflect the same chemical behavior as the $\alpha-\alpha$ correlations, the data were combined to construct a yield curve consisting of both $\alpha-\alpha$ correlation and SF-yields with better statistics.

4.3 Discussion

In Fig. 6 the combined yield curves consisting of $\alpha-\alpha$ correlation and SF-yields along with the data measured for $NbCl_5$ and $NbOCl_3$ are summarized. The yield curves were analyzed with the Monte Carlo model, assuming that two chemical species were present, namely $HaCl_5$ and $HaOCl_3$. Adsorption enthalpies of $-\Delta H_a^{0(T)}(HaOCl_3) = -117\pm3$ kJ · mol^{-1} and $-\Delta H_a^{0(T)}(HaCl_5) \geq -97$ kJ · mol^{-1} resulted, respectively. The error limits are not including systematic errors. For the volatility of $HaCl_5$ only an upper limit can be calculated, since at temperatures lower than 200 °C no data points were measured. $HaOCl_3$ becomes volatile at an approximately 50 °C higher temperature than $NbOCl_3$.

The more volatile $HaCl_5$ was formed only in a ratio of 1 : 3 compared to the less volatile $HaOCl_3$. Relativistic calculations for $HaOX_3$ (X = Cl, Br) have shown [15], that properties similar to the oxytrihalides of Nb and Ta are expected. Interestingly, Ha has the highest tendency to form a double bond with oxygen as a result of the relativistic stabilization of the 7 $s_{1/2}$(metal)-oxygen and 7 $p_{1/2}$(metal)-oxygen orbitals [15]. It is therefore conceivable that even traces of O_2 will favor the formation of the oxyhalide, compared to the pure halide. In future experiments on the volatility of $HaCl_5$ traces of O_2 and H_2O must be further reduced. One possibility would be the use of graphite columns.

The lower volatility of the oxytrihalides compared to the pentahalides can be explained by the higher ionic character and the lower covalency as well as the presence of dipole moments [15]. In order to evaluate the interaction of $MOCl_3$ (M = Nb, Ta, Ha) molecules with a dielectric surface (SiO_2) different interaction terms have to be considered. These include dipole-dipole, induction, and dispersion terms. A prediction of the relative volatility among the group 5 oxychlorides was not possible since the different contributions to the interaction energy change differently and even in opposite directions [15].

Rewriting equation (1) to

$$-\Delta H_s^{0(298)} = (1.52\pm0.10) \cdot (-\Delta H_a^{0(T)}) - (27.48\pm13.54) \quad [\text{kJ} \cdot \text{mol}^{-1}] \tag{2}$$

sublimation enthalpies can now be calculated for $HaCl_5$ and $HaOCl_3$ and compared with the predicted physicochemical properties discussed in chapter 2. In Table 5, the experimentally determined adsorption enthalpies of group 5 pentachlorides, oxytrichlorides from this work and pentabromides from [17] were converted to sublimation enthalpies using Equation (2). It was assumed that Equation (2) is applicable also for bromides. In order to allow a comparison of the adsorption- and sublimation enthalpies from this work with those from [17], the data were reanalyzed using the Monte Carlo model. The resulting, somewhat higher, adsorption and sublimation enthalpies are mainly due to a difference in τ_0 ($2 \cdot 10^{-13}$ compared to 10^{-12} in [17]). The determined sublimation enthalpies for $NbCl_5$ and $NbOCl_3$, as well as for $NbBr_5$ and $TaBr_5$ are in good agreement with the literature data. The experimental upper limit of 120 kJ · mol^{-1} for the sublimation enthalpy of $HaCl_5$ is consistent with the relativistic calculations as well as with the extrapolated values. With both methods, $HaCl_5$ is expected to be equally or more volatile than $NbCl_5$. As predicted by the classical extrapolations, we have indeed observed a less volatile $HaOCl_3$ compared to $NbOCl_3$. Unfortunately, measurements of Ta-chlorides with OLGAIII are still lacking. It would be interesting to investigate the relative volatility of the oxychlorides of group 5 and the influence of the O_2 concentration on the formation of $TaCl_5$ and $TaOCl_3$ in comparison with Nb and Ha. A $-\Delta H_s^{0(298)}$-value of 158±25 kJ · mol^{-1} was deduced for Ha-bromide. It was argued, that since the addition of BBr_3, which strongly reacts with trace amounts of O_2, didn't yield a more volatile Ha-bromide, the observed species was probably $HaBr_5$. However, this result was in contrast with theoretical calculations [14] that, as for $HaCl_5$, predicted a higher volatility compared to the lighter homologues. Since the deduced sublimation enthalpy for Ha-bromide is very similar to the value determined for $HaOCl_3$, the formation of $HaOBr_3$ in these experiments must be considered.

In this context it is also interesting to compare the different theoretical predictions for the volatility of Ha pentahalides. In fact, the predicted sublimation enthalpies differ only by about 10 to 20 kJ · mol^{-1}, which results in adsorption enthalpy differences of 6 to 14 kJ · mol^{-1}. These fairly small differences will require very precise measurements in order to clearly proof

Table 5. Experimentally determined physicochemical properties of group 5 pentachlorides, oxytrichlorides, and pentabromides compared to literature data and predicted relativistic and from periodic trends extrapolated values

Supposed species	$\Delta H_a^{0(T)}$ ($kJ \cdot mol^{-1}$)	$\Delta H_s^{0(298)a}$ (this work) ($kJ \cdot mol^{-1}$)	$\Delta H_s^{0(298)b}$ (literature) ($kJ \cdot mol^{-1}$)	$\Delta H_s^{0(298)c}$ (relativistic) ($kJ \cdot mol^{-1}$)	$\Delta H_s^{0(298)d}$ (extrapolated) ($kJ \cdot mol^{-1}$)
$NbCl_5$	-80 ± 1	95 ± 16	94.0		
$NbOCl_3$	-99 ± 1	124 ± 16	128.5		
$HaCl_5$	≥ -97	≤ 120		85	94
$HaOCl_3$	-117 ± 3	152 ± 18			180
$NbBr_5$	-93 ± 4^e	115 ± 18	112.5		
$TaBr_5$	-101 ± 4^e	127 ± 18	121.9		
Ha-bromide	-121 ± 11^e	158 ± 25		97[f]	109–118[f]

[a] Calculated using equation [2].
[b] Values from [21].
[c] Predicted values from relativistic calculations [13, 14].
[d] Extrapolated values from [20, 59].
[e] Reanalyzed experimental data from [17].
[f] Values for $HaBr_5$.

the influence of relativistic effects on the volatility of Ha halides. Also, the reliability of theoretical predictions still must be established.

Acknowledgments

The authors are indebted to the Division of Chemical Sciences, Office of Basic Energy Sciences, U.S. Department of Energy, for providing the ^{249}Bk target material available through the transplutonium element production facilities at the Oak Ridge National Laboratory.

We wish to thank the staff and crew of the LBL 88-inch Cyclotron for providing the ^{18}O beams and for technical support.

The members of the Swiss group have enjoyed the hospitality of the Lawrence Berkeley Laboratory Nuclear Science Division.

This work was supported in part by the Director, Office of Energy Research, Office of Basic Energy Sciences, Chemical Sciences Division of the U.S. Department of Energy under Contract No. DE-AC03-76SF00098.

References

1. Desclaux, J. P., Fricke, B.: J. Phys. (Paris) **41**, 943 (1980).
2. Brewer, L.: High Temp. Sci. **17**, 1 (1984).
3. Keller, Jr., O. L.: Radiochim. Acta **37**, 169 (1984).
4. Hoffman, D. C.: *Chemistry of the Transactinide Elements*, Proceedings of the Robert A. Welch Foundation Conference on Chemical Research XXXIV Fifty Years with Transuranium Elements, Houston, 255 (1990).
5. Schädel, M.: Proceedings of the International School-Seminar on Heavy Ion Physics, Dubna, 84 (1990).
6. Schädel, M.: Inst. Phys. Conf. Ser. **No. 132**, 413 (1992).
7. Türler, A., Gäggeler, H. W., Gregorich, K. E., Barth, H., Brüchle, W., Czerwinski, K. R., Gober, M. K., Hannink, N. J., Henderson, R. A., Hoffman, D. C., Jost, D. T., Kacher, C. D., Kadkhodayan, B., Kovacs, J., Kratz, J. V., Kreek, S. A., Lee, D. M., Leyba, J. D., Nurmia, M. J., Schädel, M., Scherer, U. W., Schimpf, E., Vermeulen, D., Weber, A., Zimmermann, H. P., Zvara, I.: J. Radioanal. Nucl. Chem. **160**, 327 (1992).
8. Türler, A., Gäggeler, H. W., Eichler, B., Jost, D. T., Kovacs, J., Scherer, U. W., Kadkhodayan, B., Gregorich, K. E., Hoffman, D. C., Kreek, S. A., Lee, D. M., Schädel, M., Brüchle, W., Schimpf, E., Kratz, J. V.: Proceedings of the International School-Seminar on Heavy Ion Physics, Dubna, Russia, 10–15 May 1993, 186 (1993).
9. Hoffman, D. C.: Radiochim. Acta **61**, 123 (1993).
10. Gäggeler, H. W.: J. Radioanal. Nucl. Chem. **183**, 261 (1994).
11. Kratz, J. V.: J. Alloys and Comp. **213/214**, 20 (1994).
12. Türler, A.: Radiochim. Acta **72**, 7 (1996).
13. Pershina, V., Sepp, W.-D., Fricke, B., Rosén, A.: J. Chem. Phys. **96**, 8367 (1992).
14. Pershina, V., Sepp, W.-D., Fricke, B., Kolb, D., Schädel, M., Ionova, G. V.: J. Chem. Phys. **97**, 1116 (1992).
15. Pershina, V., Sepp, W.-D., Bastug, T., Fricke, B., Ionova, G. V.: J. Chem. Phys. **97**, 1123 (1992).
16. Pershina, V., Fricke, B.: J. Phys. Chem. **98**, 6468 (1994).
17. Gäggeler, H. W., Jost, D. T., Kovacs, J., Scherer, U. W., Weber, A., Vermeulen, D., Türler, A., Gregorich, K. E., Henderson, R. A., Czerwinski, K. R., Kadkhodayan, B., Lee, D. M., Nurmia, M., Hoffman, D. C., Kratz, J. V., Gober, M. K., Zimmermann, H. P., Schädel, M., Brüchle, W., Schimpf, E., Zvara, I.: Radiochim. Acta **57**, 93 (1992).
18. Fricke, B., Johnson, E., Martinez-Rivera, G.: Radiochim. Acta **62**, 17 (1993).
19. Pershina, V., Fricke, B., Ionova, G. V., Johnson, E.: J. Phys. Chem. **98**, 1482 (1994).
20. Eichler, B., Türler, A., Gäggeler, H. W.: PSI Condensed Matter Research and Material Sciences Progress Report 1994, Villigen, Annex IIIA, Annual Report, 77 (1995), unpublished.
21. Knacke, O., Kubaschewski, O., Hesselmann, K. (Eds.).: *Thermochemical Properties of Inorganic Substances II*, Springer-Verlag, Berlin (1991).
22. Zvara, I., Belov, V. Z., Korotkin, Yu. S., Shalayevsky, M. R., Shchegolev, V. A., Hussonnois, M., Zager, B. A.: Communications of the Joint Institute for Nuclear Research, Dubna, **P12-5120** (1970).
23. Zvara, I.: Joint Institute for Nuclear Studies, Dubna, **E12-7547** (1973); contribution to XXIV International Conference on Pure and Applied Chemistry, Hamburg, Vol. 6, Radiochemistry, Butterworths, London (1973).
24. Zvara, I., Belov, V. Z., Domanov, V. P., Shalaevskii, M. R.: Radiokhimiya **18**, 371 (1976); Soviet Radiochemistry **18**, 328 (1976).

25. Zvara, I., Timokhin, S. N., Chuburkov, Yu. T., Yakushev, A. B., Gorski, B.: Joint Institute for Nuclear Research, Laboratory of Nuclear Reactions, **E7-91-75**, 36 (1991).
26. Nai-Qi, Ya, Jost, D. T., Baltensperger, U., Gäggeler, H. W.: Radiochim. Acta **47**, 1 (1989).
27. Gäggeler, H. W., Jost, D. T., Baltensperger, U., Weber, A., Kovacs, A., Vermeulen, D., Türler, A.: Nucl. Instrum. Methods **A309**, 201 (1991).
28. Gäggeler, H., Jost, D., Baltensperger, U., Ya-NaiQi, Gregorich, K. E., Gannett, C. M., Hall, H. L., Henderson, R. A., Lee, D. M., Leyba, J. D., Nurmia, M. J., Hoffman, D. C., Türler, A., Lienert, C., Schädel, M., Brüchle, W., Kratz, J. V., Zimmermann, H. P., Scherer, U. W.: Bericht Paul Scherrer Institut, Villigen, **Nr. 49** (1989), unpublished.
29. Kadkhodayan, B.: Ph.D. Thesis, Lawrence Berkeley Laboratory Report, Berkeley, **LBL-33961** (1993).
30. Türler, A., Gäggeler, H. W., Eichler, B., Jost, D. T., Kovacs, A., Vermeulen, D., Kadkhodayan, B., Gregorich, K. E., Kreek, S. A., Lee, D. M., Hoffman, D. C., Baisden, P., Kratz, J. V., Becker, H.-U., Gober, M. K., Zimmermann, H. P., Schädel, M., Brüchle, W., Jäger, E., Pershina, V., Schausten, B., Schimpf, E.: PSI Condensed Matter Research and Material Sciences Progress Report 1992, Villigen, Annex IIIA, Annual Report 95 (1993), unpublished.
31. Schwyn, S., Garwin, E., Schmitt-Ott, A.: J. Aerosol. Sci. **19**, 639 (1988).
32. Stober, J.: Diploma thesis, ETH Zürich (1988), unpublished.
33. Türler, A., Ammann, M.: PSI Condensed Matter Research and Material Sciences Progress Report 1993, Villigen, Annex IIIA, Annual Report 73 (1994), unpublished.
34. Eichler, B., Türler, A., Jost, D. T., Gäggeler, H. W.: PSI Condensed Matter Research and Material Sciences Progress Report 1993, Villigen, Annex IIIA, Annual Report 97 (1994), unpublished.
35. Hoffman, D. C., Lee, D. M., Ghiorso, A., Nurmia, M. J., Aleklett, K., Leino, M.: Phys. Rev. **C24**, 495 (1981).
36. Gregorich, K. E., Hall, H. L., Henderson, R. A., Leyba, J. D., Czerwinski, K. R., Kreek, S. A., Kadkhodayan, B. A., Nurmia, M. J., Lee, D. M., Hoffman, D. C.: Phys. Rev. **C45**, 1058 (1992).
37. Zvara, I.: Radiochim. Acta **38**, 95 (1985).
38. Türler, A., Gregorich, K. E., Hoffman, D. C., Lee, D. M., Gäggeler, H. W.: PSI Condensed Matter Research and Material Sciences Progress Report 1991, Villigen, Annex III, Annual Report 68 (1992), unpublished.
39. Eichler, B., Reetz, T., Domanov, V. P.: Report JINR, Dubna, **P12-20047** (1976).
40. Eichler, B., Domanov, V. P., Zvara, I.: Report JINR, Dubna, **P12-9454** (1976).
41. Rudolph, J., Bächmann, K.: Microchim. Acta **I**, 477 (1979).
42. Rudolph, J., Bächmann, K.: J. Radioanl. Chem. **43**, 113 (1978).
43. Rudolph, J., Bächmann, K.: Radiochim. Acta **27**, 105 (1980).
44. von Dincklage, R. D., Schrewe, U. J., Schmidt-Ott, W. D., Fehse, H. F., Bächmann, K.: Nucl. Instrum. Methods **176**, 529 (1980).
45. Domanov, V. P., Zin, Kim U.: Radiokhimiya **31**, 19 (1989).
46. Bruchertseifer, F., Türler, A., Eichler, B., Gäggeler, H. W., Jost, D. T.: PSI Condensed Matter Research and Material Sciences Progress Report 1993, Villigen, Annex IIIA, Annual Report, 105 (1994), unpublished.
47. Schädel, M., Brüchle, W., Schimpf, E., Zimmermann, H. P., Gober, M. K., Kratz, J. V., Trautmann, N., Gäggeler, H., Jost, D., Kovacs, J., Scherer, U. W., Weber, A., Gregorich, K. E., Türler, A., Czerwinski, K. R., Hannink, N. J., Kadkhodayan, B., Lee, D. M., Nurmia, M. J., Hoffman, D. C.: Radiochim. Acta **57**, 85 (1992).
48. Ghiorso, A., Nurmia, M., Eskola, K., Eskola, P.: Phys. Rev. **C4**, 1850 (1971).
49. Gregorich, K. E., Henderson, R. A., Lee, D. M., Nurmia, M. J., Chasteler, R. M., Hall, H. L., Bennett, D. A., Gannett, C. M., Chadwick, R. B., Leyba, J. D., Hoffman, D. C.: Radiochim. Acta **43**, 223 (1988).
50. Kratz, J. V., Zimmermann, H. P., Scherer, U. W., Schädel, M., Brüchle, W., Gregorich, K. E., Gannett, C. M., Hall, H. L., Henderson, R. A., Lee, D. M., Leyba, J. D., Nurmia, M. J., Hoffman, D. C., Gäggeler, H., Jost, D., Baltensperger, U., Ya-NaiQi, Türler, A., Lienert, C.: Radiochim. Acta **48**, 121 (1989).
51. Zimmermann, H. P., Gober, M. K., Kratz, J. V., Schädel, M., Brüchle, W., Schimpf, E., Gregorich, K. E., Türler, A., Czerwinski, K. R., Hannink, N. J., Kadkhodayan, B., Lee, D. M., Nurmia, M. J., Hoffman, D. C., Gäggeler, H., Jost, D. T., Kovacs, J., Scherer, U. W., Weber, A.: Radiochim. Acta **60**, 11 (1993).
52. Kratz, J. V., Gober, M. K., Zimmermann, H. P., Schädel, M., Brüchle, W., Schimpf, E., Gregorich, K. E., Türler, A., Hannink, N. J., Czerwinski, K. R., Kadkhodayan, B., Lee, D. M., Nurmia, M. J., Hoffman, D. C., Gäggeler, H., Jost, D. T., Kovacs, J., Scherer, U. W., Weber, A.: Phys. Rev. **C45**, 1064 (1992).
53. Bemis, Jr., C. E., Ferguson, R. L., Plasil, F., Silva, R. J., O'Kelly, G. D., Kiefer, M. L., Hahn, R. L., Hensley, D. C., Hulet, E. K., Lougheed, R. W.: Phys. Rev. Lett. **39**, 1246 (1977).
54. Bemis, Jr., C. E., Ferguson, R. L., Silva, R. J., Plasil, F., O'Kelly, G. D., Hahn, R. L., Hensley, D. C., Hulet, E. K., Lougheed, R. W.: Bulletin of the American Physical Society **22**, 611 (1977).
55. Druin, V. A., Bochev, B., Lobanov, Yu. V., Sagaidak, R. N., Kharitonov, Yu. P., Tret'yakova, S. P., Gul'bekyan, G. G., Bulkanov, G. V., Erin, E. A., Kosyakov, V. N., Rykov, A. G.: Sov. J. Nucl. Phys. **29**, 591 (1979).
56. Welch, R. B., Gyger, F., Jost, D. T., von Gunten, H. R., Krähenbühl, U.: Nucl. Instrum. Methods **A269**, 615 (1988).
57. Gregorich, K. E.: Nucl. Instrum. Methods **A302**, 135 (1991).
58. Gäggeler, H., Jost, D., von Gunten, H. R.: Technische Mitteilung, Villigen, **TM-44-87-04** (1987), unpublished.
59. Eichler, B.: PSI Condensed Matter Research and Material Sciences Progress Report 1993, Villigen, Annex IIIA, Annual Report 93 (1994), unpublished.